Cell, Vol. 89, 875–886, June 13, 1997, Copyright ©1997 by Cell Press

# Structural and Functional Analysis of the Mitotic Rotamase Pin1 Suggests Substrate Recognition Is Phosphorylation Dependent

**Rama Ranganathan,*§ Kun Ping Lu,†‡**
**Tony Hunter,† and Joseph P. Noel***
*Structural Biology Laboratory
†Molecular Biology and Virology Laboratory
The Salk Institute for Biological Studies
La Jolla, California 92037
‡Cancer Biology Program
Division of Hematology/Oncology
Department on Medicine
Beth Israel Deaconess Medical Center
and Division of Aging
Harvard Medical School
Boston, Massachusetts 02215

## Summary

**The human rotamase or peptidyl-prolyl *cis-trans* isomerase Pin1 is a conserved mitotic regulator essential for the G2/M transition of the eukaryotic cell cycle. We report the 1.35 Å crystal structure of Pin1 complexed with an AlaPro dipeptide and the initial characterization of Pin1's functional properties. The crystallographic structure as well as pH titration studies and mutagenesis of an active site cysteine suggest a catalytic mechanism that includes general acid-base and covalent catalysis during peptide bond isomerization. Pin1 displays a preference for an acidic residue N-terminal to the isomerized proline bond due to interaction of this acidic side chain with a basic cluster. This raises the possibility of phosphorylation-mediated control of Pin1–substrate interactions in cell cycle regulation.**

## Introduction

The eukaryotic cell cycle is characterized by defined periods of preparation for chromosome replication (G1), DNA replication (S), preparation for mitosis (G2), and mitosis (M). Proper transitions between these states require an evolutionarily conserved set of protein kinases that include the cyclin-dependent kinases (CDKs) (reviewed in Nurse, 1994; King et al., 1994). The overall principle underlying cell cycle regulation is the appropriately timed structural modification of proteins through phosphorylation/dephosphorylation, and ubiquitin-mediated protein degradation. For example, the G2/M transition in all eukaryotic cells requires CDC2, a protein-serine/threonine kinase with catalytic specificity for prolines immediately C-terminal to the phosphorylation site. CDC2 activity requires the association of cyclin B; the activity of cyclin B/CDC2 is negatively regulated by phosphorylation by the Wee1 and Myt1 protein kinases, and positively regulated by the dephosphorylation of Thr-14 and Tyr-15 by the CDC25C phosphatase (King et al., 1994). Cyclin B is expressed starting at the end of the S phase and must be degraded in a ubiquitin-dependent manner for exit from mitosis. A central step in understanding the biology of cell cycle regulation is the study of the structural basis for these regulatory modifications that control cell cycle transitions.

The NIMA protein kinase is essential for mitosis in Aspergillus nidulans (Osmani et al., 1991; Lu and Means, 1994), and a NIMA-like pathway is also required for the G2/M transition in vertebrate cells (Lu and Hunter, 1995). Using a yeast two-hybrid screen, three human proteins, Pin1–3, were identified that interact with NIMA and suppress the NIMA-induced lethal phenotype in yeast (Lu et al., 1996). The properties of Pin1 and its budding yeast homolog, Ess1, suggest that they act as regulators of mitosis (Lu et al., 1996). Pin1 is a 163 amino acid polypeptide with an N-terminal 39-residue WW domain, a putative protein–protein interaction motif, and a C-terminal rotamase (peptidyl-prolyl *cis-trans* isomerase-PPIase) domain (Lu et al., 1996). Depletion of Pin1 in HeLa cells or Ess1 in yeast cells results in mitotic arrest, while overexpression of Pin1 in HeLa cells causes G2 arrest. Human Pin1 complements an *ess1*$^-$ yeast mutant, a finding that highlights the degree of evolutionary conservation of the Pin1-dependent regulatory system. Pin1 is exclusively nuclear and is a component of the nuclear speckle, a large macromolecular complex that includes several cell cycle proteins as well as some components of the splicing machinery. Pin1 regulation of the G2/M transition probably involves interactions with the NIMA kinase and/or other cell cycle regulatory proteins.

The N-terminal WW domain of Pin1 is a small structural motif that has been recognized in many functionally and evolutionarily diverged proteins. Like SH3 domains, the WW domain acts as a protein interaction module that binds to short proline-rich segments of target proteins (reviewed in Sudol, 1996a; Staub and Rotin, 1996). Defining characteristics of the WW domain are the presence of two invariant tryptophans, one near each terminus, a proline near the C terminus, and a cluster of aromatic residues located centrally in the primary sequence (see Figure 1A). Hypotheses for WW domain function in Pin1 include substrate recognition, interaction with anchoring proteins for subcellular localization, and/or facilitation of nuclear import.

The C-terminal domain of Pin1 encodes an essential PPIase domain (Lu et al., 1996), whose enzymatic activity and substrate specificity suggests a novel mechanism for the regulation of cell cycle proteins. PPIases are ubiquitous enzymes that catalyze rotation about the peptide bond preceding a proline and may accelerate the folding and trafficking of some proteins (Schmid, 1995). There are three structurally distinct PPIase subfamilies: the cyclosporin A–binding proteins (cyclophilins), the FK506-binding proteins (FKBPs), and a more recently described third class that includes the E. coli protein parvulin and related bacterial proteins, the product of the *dodo* gene from Drosophila and Pin1/Ess1. Although little is known about the parvulin/Pin1 class, the first two classes of PPIases have been extensively

§Present Address: Howard Hughes Medical Institute, UT Southwestern Medical Center, Dallas, Texas 75235.

characterized because of their importance as cellular targets of clinically relevant immunosuppressants. Interestingly, the immunosuppressive property of the drug/isomerase complexes is unrelated to inhibition of the PPIase activity, and indeed, evidence for the biological importance of this enzymatic activity is limited. In this regard, the requirement for Pin1/Ess1 PPIase activity (Lu et al., 1996) during cell cycle progression provides an excellent opportunity to study the biological mechanism of PPIase activity. We now report the X-ray crystal structure of human Pin1 complexed with an AlaPro dipeptide at 1.35 Å resolution, and an initial characterization of its functional properties. This structure suggests a novel mechanism of peptidyl-prolyl bond isomerization and a unique selectivity for the residue on the N-terminal side of the proline, findings that have important implications for cell cycle regulation.

## Results

### Crystallization and Structure Determination

Human Pin1 was expressed as an N-terminal histidine-tagged fusion protein in E. coli, purified by $Ni^{2+}$ chelation and size exclusion chromatography, crystallized, and its structure solved as described in Experimental Procedures. The final model contained 208 water molecules, one sulfate ion, one AlaPro dipeptide (*cis* configuration), and two PEG400 molecules and yielded a free R factor of 26.6% for 5% of the data (no sigma cutoff) between 6.0 Å and 1.35 Å resolution. The Ramachandran plot showed no outliers (Table 1).

### Overall Architecture and Domain Topology

Pin1 consists of two structural domains organized around a hydrophobic cavity. The N-terminal WW domain, residues 1–39, consists of a triple-stranded antiparallel β sheet. An approximate 90° twist in the lower portion of the β sheet relative to the upper portion and a downward bend in the upper half of the WW domain form a deep hydrophobic concave surface that comprises one wall of the hydrophobic cavity (Figure 1A). The hydrophobic wall of the WW domain sequesters a PEG molecule, with the Tyr-23/Trp-34 aromatic pair clamping down upon the PEG molecule while Ser-16 and Ser-32 extend this clamp in either direction (Figure 1B). Spatially, this PEG molecule forms a continuous path through the interdomain cavity exiting out of a narrow opening on the backside of Pin1.

The C-terminal PPIase domain, residues 45–163, forms the opposing wall of the interdomain cavity. In particular, a scaffolding alpha helix, α1, contributes a total of 9 residues to this wall and creates a 23 Å deep internal surface opposite the WW domain's hydrophobic pocket (Figure 1B). Notably, this helical insertion into the core PPIase fold is found only in the PPIase domains of Pin1, Ess1, and Dodo that possess N-terminal WW

Table 1. Summary of Crystallographic Data

Data Collection Statistics

| Data Set | Source | Resolution Limit (Å) | Reflections Measured (Unique) | Completeness All/Outer Shell | Rsym (%)[a] All/Outer Shell | $<I/\sigma>$ All/Outer Shell | Heavy Atom Sites |
|---|---|---|---|---|---|---|---|
| Nat I | Salk | 2.05 | 11139 | 99.7/99.9 | 6.7/45.3 | 21/4 | — |
| AP II | SSRL 7-1 | 1.35 | 33672 | 95.5/69.0 | 5.3/59.2 | 18/2 | — |
| TAMM I | Salk | 2.5 | 9751[b] | 87.8/87.7 | 5.8/22.2 | 14/5 | ''1'' |
| PIP I | Salk | 2.5 | 10986[b] | 99.4/98.5 | 6.6/35.3 | 19/4 | ''5'' |

Multiple Isomorphous Replacement with Anomalous Scattering Statistics

| Resolution (Å) | 20–10.54 | 7.07 | 5.42 | 4.39 | 3.70 | 3.19 | 2.81 | 2.50 | Overall |
|---|---|---|---|---|---|---|---|---|---|
| Phasing power[c] | | | | | | | | | |
| TAMM Isomorphous | 1.52 | 1.57 | 2.26 | 1.85 | 1.35 | 1.26 | 1.43 | 1.35 | 1.46 |
| TAMM Anomalous | 0.84 | 0.90 | 0.88 | 0.71 | 0.50 | 0.42 | — | — | 0.63 |
| PIP Isomorphous | 1.46 | 1.71 | 2.10 | 1.76 | 1.44 | 1.51 | 1.70 | 1.66 | 1.64 |
| PIP Anomalous | 1.00 | 0.92 | 1.03 | 0.84 | 0.66 | 0.50 | 0.39 | — | 0.63 |
| Mean figure of merit[d] | 0.66 | 0.67 | 0.73 | 0.69 | 0.59 | 0.53 | 0.51 | 0.45 | 0.54 |

Refinement Statistics

| Data set | Resolution Range (Å) | R factor[e] | Free R factor[e] | Unique Reflections (working/test)[e] |
|---|---|---|---|---|
| Nat I | 6.00–2.05 | 25.6 | 31.2 | 10090/505 |
| AP II | 6.00–1.35 | 22.3 | 26.6 | 31532/1678 |
| 17.8 main chain (AP II) | 1.0 main chain (AP II) | | 0.005 (Nat I) | 1.39 (Nat I) |
| 22.8 side chain (AP II) | 2.0 side chain (AP II) | | 0.008 (AP II) | 1.78 (AP II) |
| Average B factor (Å$^2$) | B factor RMSD (Å$^2$) | | Bond length RMSD (Å) | Bond angle RMSD (°) |

[a] $Rsym = \Sigma_h|I_h - <I_h>|/\Sigma_h I_h$ where $<I_h>$ is the average intensity of reflection h for its symmetry and Friedel equivalents.

[b] Friedel pairs were not merged. Therefore, the number of unique and measured reflections reflects this nonequivalence.

[c] Phasing power $= \Sigma|F_h^c|\Sigma|||F_p^o|\exp(i\varphi_c) + F_h^c| - |F_{ph}^o||$, where $F_h^c$ = heavy-atom structure factor, and $|F_p^o|$ and $|F_{ph}^o|$ are observed amplitudes for the protein and heavy-atom derivatives respectively, and $\varphi_c$ is the experimental phase.

[d] Figure of merit $= \int P(\varphi)\exp(i\varphi)d\varphi/\int P(\varphi)d\varphi$, where P is the probability distribution of φ, the phase angle.

[e] R factor $= \Sigma_h(|F_o(h) - F_c(h)|)/\Sigma_h F_o(h)$, where $F_o(h)$ and $F_c(h)$ are the observed and calculated structure factor amplitudes for reflection h, respectively. The Free R factor is calculated in an analogous manner for 5% of the data that has never been used for refinement. The R factor is calculated with the remaining 95% of the measured data. Both values are calculated with no sigma cutoff.

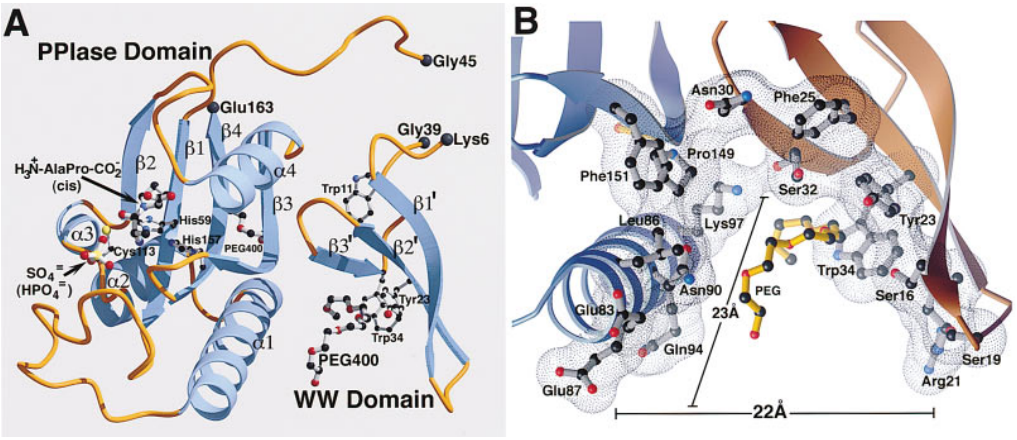


Figure 1. Overall Fold of Human Pin1

(A) Ribbon representation of Pin1. Residues 1–6 and 40–44 are not visible in electron density maps and are disordered. Apostrophes distinguish the WW domain secondary structural elements from the PPIase domain's secondary structural features. Atoms are color coded for clarity (oxygen is red, nitrogen is blue, carbon is black, and sulfur is yellow). The $HPO_4^{2-}$ label reflects the possible substitution of sulfate by phosphate in phosphate-soaked crystals. Produced with MOLSCRIPT (Kraulis, 1991) and Raster3D (Bacon and Anderson, 1988).

(B) Ribbon and molecular surface representation of the Pin1 interdomain cavity. View is the same as in (A). The WW domain is orange and the PPIase domain is light blue. The dotted surface depicts the solvent-accessible surface for residues lining the interdomain cavity. The cavity presents a largely hydrophobic composite surface as indicated by the predominance of carbon atoms lining the cavity. Produced with RIBBONS (Carson and Bugg, 1986).

domains (see Figure 4). The conservation of this structural element on the surface of the Pin1 PPIase's interdomain cavity suggests that α1 plays a functional role in the Pin1 subfamily of dual domain PPIases as one element in a composite protein–protein interface. Residues in the β2′/β3′ loop (WW domain), β3′ (WW domain), α1 (PPIase), α4 (PPIase), and the middle portion of β3 (PPIase) constitute the highly ordered interaction surface linking the WW and PPIase domains.

The overall fold of the Pin1 WW domain is similar to the reported NMR solution structure of the isolated YAP65 WW domain (Macias et al., 1996) (Figures 2A and 2B). The YAP65 WW domain binds to proline-rich peptides with a consensus sequence, PPxY, in vitro (Sudol et al., 1995; Staub and Rotin, 1996) and competes with the formin-binding protein SH3 domains for ligand binding (Chan et al., 1996; Sudol, 1996b). The YAP65 WW domain structure complexed with a peptide containing the PPxY motif contacts the terminal peptide tyrosine (Tyr7′) via Leu-190(30) and His-192(32) of the WW domain (see lower panel, Figure 2A). The limited contact surface provides little insight into the mechanisms underlying polyproline specificity. Leu-190(30) and His-192(32) of the YAP65 WW domain are structurally equivalent to Phe-25 and His-27, respectively, of the Pin1 WW domain. A possibility is that, like in Pin1, other WW domains contribute one structural component to a composite protein interaction surface. Substrate specificity may depend on the summed contributions of all the participating structural elements.

The central scaffolding of the C-terminal PPIase domain consists of a four-stranded anti-parallel β sheet. In addition, four alpha helices surround the flattened half β barrel. A set of absolutely conserved catalytic residues in the Pin1/Ess1 class of PPIase project outward from the barrel structure and define the binding pocket for the proline (Leu-122, Met-130, Phe-134) and the peptide bond that undergoes *cis*/*trans* isomerization. Also, a triad of basic side chains consisting of Lys-63, Arg-68, and Arg-69 cluster in the lower portion of the active site and sequester a crystallographically well ordered sulfate ion (middle panels, Figures 3A and 3B). The spatial proximity of this tripartite basic cluster in the active site to the bound dipeptide suggests that this anionic recognition site confers preferential binding to substrates with an acidic residue N-terminal to the proline.

Despite the lack of primary sequence similarity with the other two structural classes of PPIase (FKBP-like and cyclophilin-like), the core β sheet and the α4 helix of the Pin1 PPIase domain fold in a similar fashion to FKBP (Figure 3A). However, we find that active site residues of Pin1 and FKBP diverge significantly, suggesting at least partial differences in the catalytic mechanism (Figures 3B and 4).

### An Analysis of Pin1 Surface Properties

In addition to the hydrophobic clusters within the PPIase domain's active site and the interdomain cavity, a group of four conserved and surface-exposed residues define a third solvent-accessible hydrophobic patch on Pin1. On the backside of the PPIase domain, Ile-96, Phe-103, Met-146, and Leu-160 delineate a shallow hydrophobic cleft that sequesters a second PEG400 molecule (Figure 5A). Given that solvent-exposed hydrophobic patches are generally energetically disfavored in proteins and are often maintained due to functional necessity, these hydrophobic clusters are likely relevant for Pin1 function.

Clusters of hydrophobic residues are predicted structural features of protein–protein interaction surfaces (Janin and Chothia, 1990; Clackson and Wells, 1995), and indeed, a comprehensive analysis of many such interfaces shows that they are highly correlated with the

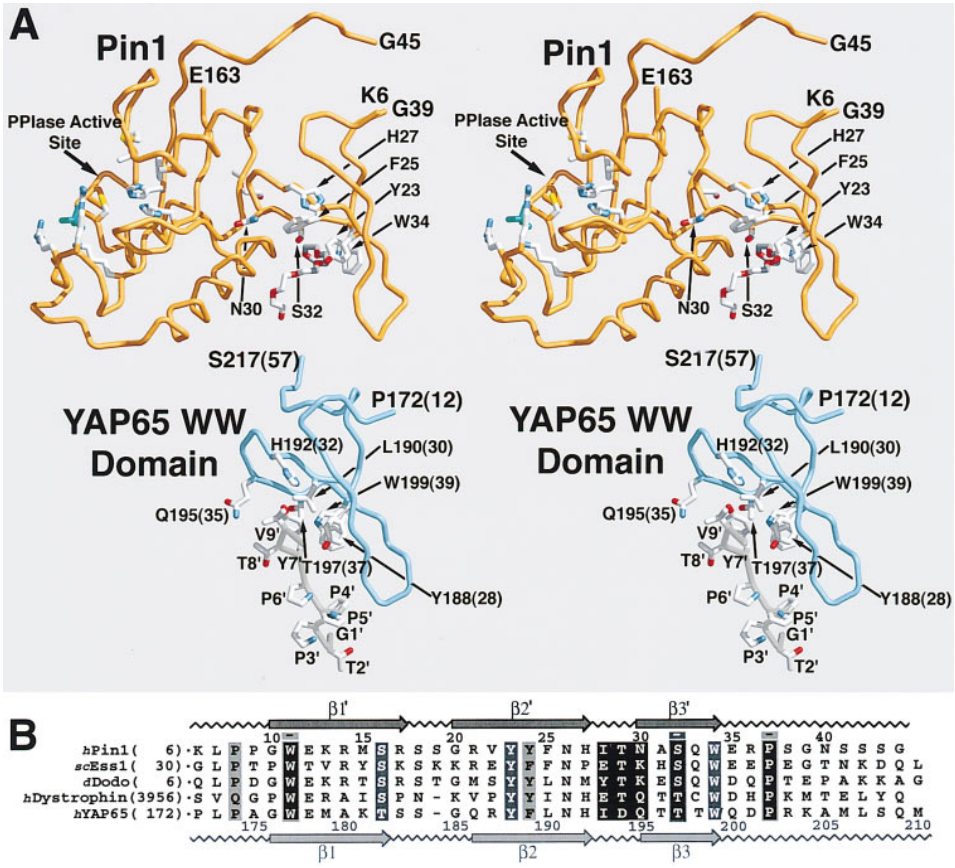


Figure 2. Comparison of the Pin1 and the YAP65 WW Domains

(A) Cα stereo view of the X-ray-derived Pin1 coordinates aligned with the NMR-derived YAP65 WW domain coordinates (Macias et al., 1996). The offset of the structures facilitates viewing. A least squares alignment of the backbone atoms for 34 homologous residues resulted in an rmsd of 2.27 Å. The residues depicted correspond to residues originally illustrated by Macias et al. (1996). The numbering scheme for YAP65 refers to the human sequence (accession number P46937). The numbers in parentheses correspond to the alternative numbering scheme of Macias et al. (1996). The atoms shown are color coded for clarity as in Figure 1, except that carbon is now light gray. Produced with the conic option (Huang et al., 1991) of MIDAS (Ferrin et al., 1988).

(B) Sequence alignment of five representative WW domains. The top and bottom lines illustrate the structural elements observed in Pin1 and YAP65 (Macias et al., 1996), respectively. The top and bottom numbering schemes refer to Pin1 and YAP65, respectively. The numbers in parentheses correspond to the first residue on each line for each of the five WW domains. Gray boxes with white letters delineate residues in direct contact with PEG400 in the case of Pin1. Black boxes with white letters define residues serving as structural links between the WW domain and the PPIase domain of Pin1. Black letters in gray boxes highlight residues that contribute to the WW domain fold. ([h] is human, [sc] is Saccharomyces cerevisiae, and [d] is Drosophila. Accession numbers: hPin1, U49070; scEss1, P22696; dDodo, U35140; hDystrophin, P11532; and hYAP65, P46937.)

degree of surface-exposed hydrophobicity (Young et al., 1994). An inference from these data is that the distribution of hydrophobicity on the solvent-accessible surface of a protein should reveal potential protein interaction sites, particularly when weighted by conservation among functionally related but evolutionarily distant homologs. To apply these principles to Pin1, we calculated a parameter $\alpha$ for each residue of Pin1 that measures the degree of functionally conserved, surface-exposed hydrophobicity. The analysis of the distribution of $\alpha$ over the Pin1 molecular surface (Figure 5B) exhibits three important features. First, the majority of the surface is expectedly low scoring (75% of residues with $\alpha < 0.05$), consistent with the prediction that high $\alpha$ scores are generally disfavored. Second, the three hydrophobic surface patches that comprise the PPIase active site and the two PEG binding sites score highly in this analysis, meeting the expected criteria for protein association domains. Finally, a path of conserved hydrophobicity can be traced on the Pin1 molecular surface that links the three surface patches into a continuous hydrophobic surface connecting the highly conserved residues of the WW domain with the PPIase domain active site via the second PEG binding site along the back of the PPIase domain $\beta$ barrel. This analysis suggests that the Pin1 active site interacts with substrates using an extended recognition surface that includes the WW domain, a proposal testable through mutagenesis of these high-scoring surface residues, and through structural studies of substrate complexes.

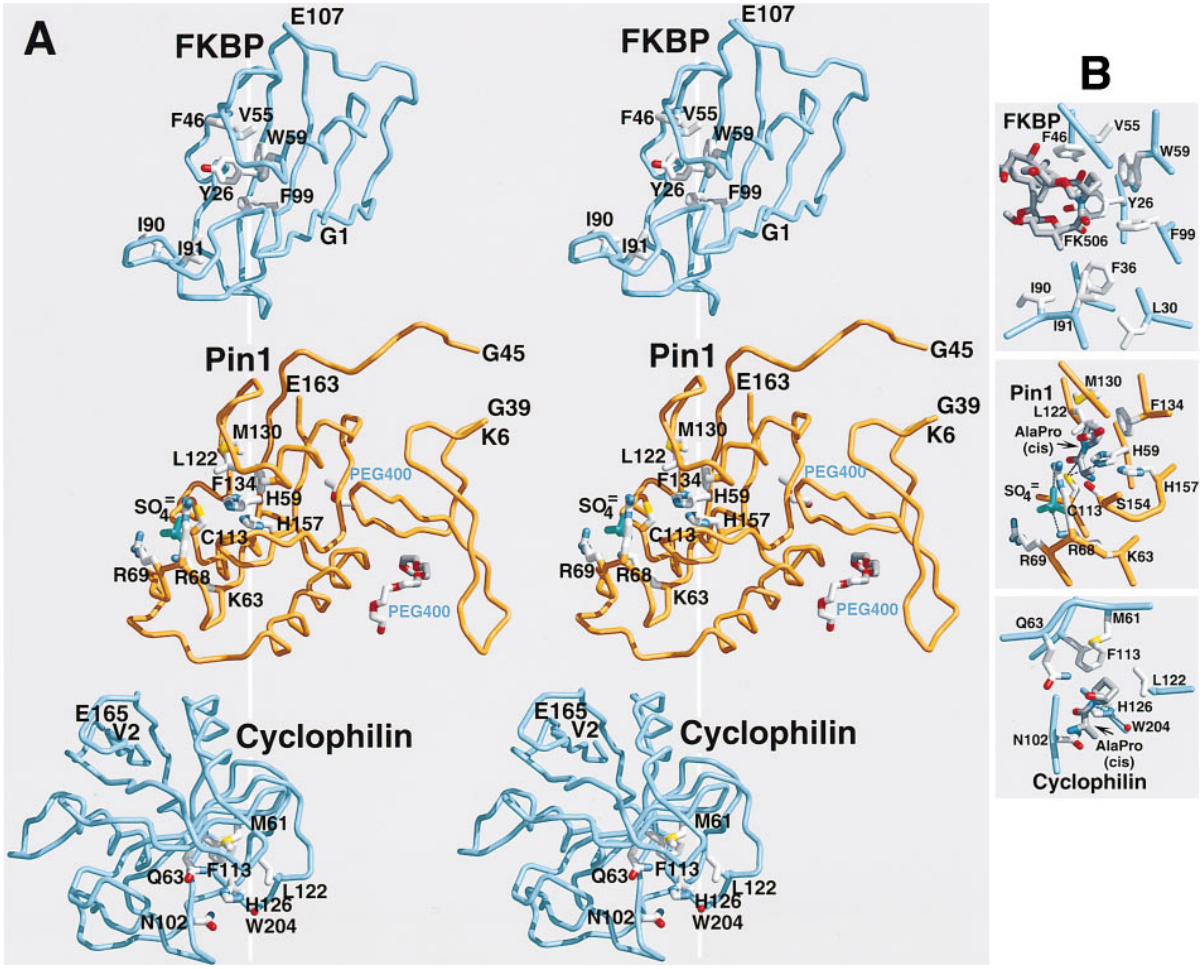


Figure 3. Structural Comparison of Representative PPIases

(A) Cα stereo pair of FKBP (PDB code 1FKF), Pin1, and cyclophilin (PDB code 1CYH) aligned and offset. The backbone atoms of Pin1 and FKBP were aligned in O (Jones et al., 1991). Pin1 and cyclophilin (CyPA) were aligned by superimposing the backbone atoms of the *cis* AlaPro dipeptides. Active site residues are shown and color coded for clarity. The white line serves as a visual clue for the aligned active sites.

(B) Active site views. A portion of FK506 bound to FKBP, and the AlaPro dipeptides bound to Pin1 and CyPA are shown. The psi (ψ) rotation for the alanine in the dipeptide bound to Pin1 relative to the same alanine in the dipeptide bound to CyPA likely occurs to avoid a steric clash between the β-methyl group of alanine and the bound sulfate anion. In Pin1, dashed gray lines emphasize the relationship of Cys-113 and His-59 to the peptide bond of the AlaPro peptide. Both panels were produced with the conic option (Huang et al., 1991) of MIDAS (Ferrin et al., 1988).

**Relationship to Other PPIases**

FKBPs and cyclophilins belong to distinct structural classes of PPIases. Despite the global similarity of the Pin1 core PPIase domain (defined in Pin1 by the secondary structural elements, β1, β2, β3, β4, and α4) to the FKBP-like class of PPIase (Figure 3A, root mean square derivation [rmsd] in homologous backbone atoms of 4.57 Å), significant structural differences exist between these two PPIase families that are likely to have important functional consequences for active site specificity and rotamase activity.

In human FKBP, the N-terminal segment forms a β strand that pairs with a strand analogous to β3 in Pin1, extending the core β barrel by one strand. In contrast, the N-terminal portion of the Pin1 PPIase domain (residues 45–53) extends over the top of the domain and covalently tethers the PPIase domain to the N-terminal WW domain through a glycine-rich linker. Indeed, Pin1's β3 strand contributes 3 of its 10 residues to the PPIase domain's interdomain interaction surface with the WW domain. A second structural deviation occurs between residues 64 and 119 of Pin1, which form the polypeptide segment linking β1 to β2. This segment includes the β1/α1 loop, α1, the α1/α2 loop, α2, the α2/α3 loop, and α3. In FKBP, the corresponding region is considerably shorter, spanning a total of 12 residues that form an additional β strand. This large structural inclusion unique to the Pin1 subfamily of this PPIase class contributes four structural motifs to the C-terminal PPIase domain that are likely to have functional roles: (1) the α1 helix that provides much of the composite hydrophobic surface shared with the WW domain, (2) residues from the α1/

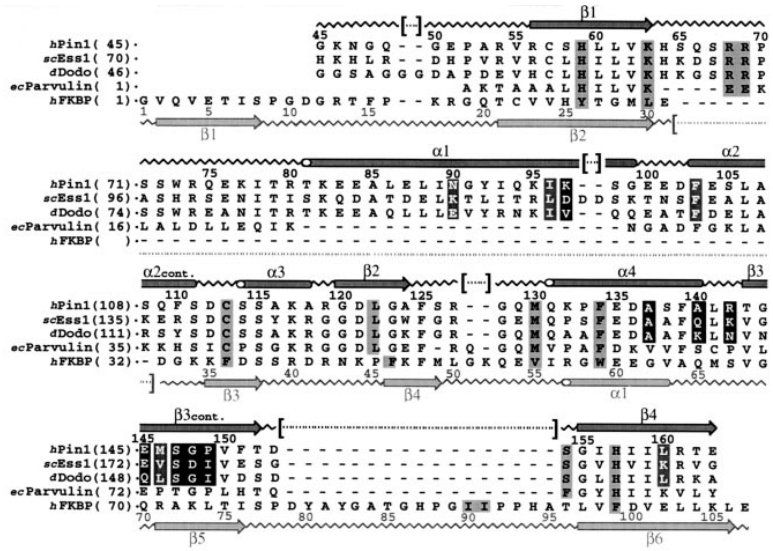


Figure 4. Sequence Alignment of Five Representative PPIase Domains

The top and bottom lines illustrate the structural elements observed in Pin1 and FKBP (Van Duyne et al., 1993), respectively. The top and bottom numbering schemes refer to Pin1 and FKBP, respectively. Numbers in parentheses correspond to the first residue on each line for each of the five PPIases. Dashed lines indicate gaps. Gray boxes with black letters delineate the active site residues. White letters in gray boxes highlight residues contributing to Pin1's PEG binding sites. Black boxes with white letters define residues serving as structural links between the PPIase domain and the WW domain. ([h] is human, [sc] is Saccharomyces cerevisiae, [d] is Drosophila, and ec is E. coli. Accession numbers: hPin1, U49070; scEss1, P22696; dDodo, U35140; ecParvulin, S48658; and hFKBP12, P20071.)

α2 loop and α2 that comprise part of the conserved second PEG binding site, (3) the multivalent anion binding site consisting of Lys-63, Arg-68, and Arg-69, and (4) an active site cysteine (Cys-113) that we propose is crucial for efficient catalysis in Pin1. Below, we use these structural observations as the basis for functional studies of Pin1 substrate specificity and catalytic mechanism.

## Substrate Specificity

The N-terminal half of the large β1/α1 loop organizes a basic cluster consisting of Lys-63, Arg-68, and Arg-69 at the entrance to the Pin1 PPIase domain's active site (Figure 3B). The conserved triad sequesters a sulfate ion in close proximity to the β methyl group of the alanine residue in the bound AlaPro dipeptide. The basic patch, its associated counterion, and the nearby AlaPro dipeptide immediately suggested that Pin1 possesses a strong preference for acidic side chains in the residue N-terminal to proline in substrates. Indeed, a glutamate or a phosphoserine (P.Ser) or P.Thr side chain modeled on the Ala of the AlaPro dipeptide superimposes its respective anionic group, carboxylate or phosphate, on the bound sulfate ion in the complex crystal structure (Figure 6A). In vitro PPIase assays using a series of tetrapeptide substrates of the form succinyl-Ala$Xaa_{i-1}$-$Pro_i$Phe-(p)-nitroanilide, where Xaa varies, confirm this hypothesis (Figure 6B). The greater than 100-fold preference for Glu at the i-1 position over Gln illustrates the specificity displayed by Pin1.

The presence of a net +3 charge around the sulfate ion argues for multiple compensatory negative charges on substrates when the Pin1 active site is engaged with biologically relevant targets. In light of the multivalent nature of the bound sulfate ion, we propose that Pin1 will preferentially catalyze isomerization of peptide bonds involving a minimal segment consisting of a P.Ser or P.Thr residue N-terminal to proline. This -SP- or -TP- motif is particularly relevant for cell cycle control since the known specificity of the CDKs, including CDC2, is for -SP- or -TP- in a variety of CDK targets. Titration of Pin1 with inorganic phosphate fully inhibited isomerase activity with apparent 1:1 stoichiometry ($K_i$ 33 mM, Figure 6C), indicating that the multivalent anion binding site is necessary for catalytic activity. Synthetic tetrapeptide substrates containing P.Ser (or P.Thr) in the i-1 position will be needed to test the selectivity of Pin1 for phosphorylated substrates.

This Pin1 substrate specificity mechanism also provides a structural explanation for the substrate specificities of FKBP and cyclophilin at the i-1 position relative to proline (Harrison and Stein, 1990b). In FKBP, the replacement of hydrophobic residues (Ile-90, Ile-91, Phe-36, Figure 3B) at the spatially analogous positions of the basic cluster in Pin1 can explain its preference for hydrophobic residues N-terminal to proline in peptide substrates. Interestingly, though Ile-90 and Ile-91 in FKBP superimpose on Pin1's basic patch in the three-dimensional structure, these residues arise from different primary sequence positions. This finding is consistent with the conservation of this structural motif as a selectivity filter for side chains at the i-1 position. In addition, cyclophilin's lack of any specificity at this position when acting upon tetrapeptide substrates is consistent with the absence of any analogous structural motif for substrate selection in this subfamily of PPIases (Figure 3B). Note that this discussion of substrate selectivity at the i-1 position focuses entirely on catalytic efficiency (measured as $k_{cat}/K_m$) against substrate peptides, and not for the overall binding energy ($K_d$) against natural protein targets. For example, the interaction of human cyclophilin A with the HIV-1 capsid protein shows significant binding specificity for the *trans* conformation of GlyPro at the active site due to energetically favorable interactions made with amino acids lying both N- and C-terminal to these residues (Gamble et al., 1996).

## Reaction Mechanism

A hydrophobic pocket composed of the residues Phe-134, Met-130, and Leu-122 forms the binding site for the cyclic side chain of the substrate proline, and the

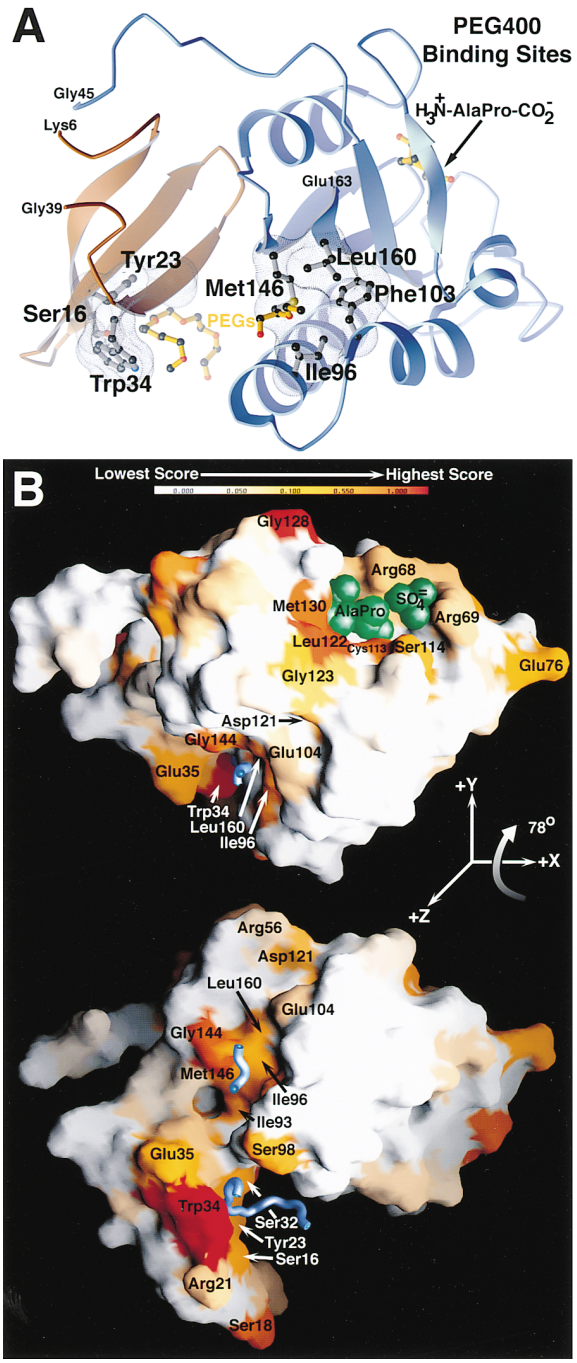


Figure 5. Pin1 Solvent-Accessible Surface

(A) Backside view relative to Figure 1A, highlighting side chains and their associated van der Waals surfaces involved in binding the two polyethylene glycol molecules (PEGs). A solvent-exposed hydrophobic surface partly defined by highly conserved residues of the WW domain, Tyr-23, Trp-34, Ser-16, and Ser-32 closely interacts with one PEG molecule, while a second hydrophobic surface comprised of Ile-96, Phe-103, Met-146, and Leu-160 from the PPIase domain binds the other PEG. The WW domain is colored orange, PPIase domain is light blue, and atoms are colored according to type. Produced with RIBBONS (Carson and Bugg, 1986).

(B) Quantitative analysis of Pin1 surface properties. The figure shows a color-coded representation of the distribution of a calculated parameter $\alpha$ that describes the degree of conserved, solvent-exposed hydrophobicity. $\alpha$ values range from 0 (white) to 1 (red), where the highest values are scored by identical, fully exposed hydrophobic residues. Produced with CCP4 and GRASP (Nicholls et al., 1991).

peptidyl-prolyl bond undergoing catalyzed isomerization is surrounded by side chains of residues Cys-113, His-59, His-157, and Ser-154 (Figure 3B). These latter residues are symmetrically distributed around the bond rotation axis and, as described below, are placed to make conformation-specific interactions with the substrate during isomerization. Finally, as discussed above, the basic residues Lys-63, Arg-68, and Arg-69 are sequestered in a cluster near the i-1 substrate residue and mediate catalytic selectivity for the side chain N-terminal to the proline (Figures 3B and 6B).

Rotation around peptide bonds is energetically disfavored due to their partial double-bond character; this is due to delocalization of the lone-pair electrons of the amide nitrogen in the ground state that results in a polar resonance species with planar geometry. This property results in a ~22 kcal/mol energy barrier to rotation, and restrains the peptide bond in either *cis* ($\omega = 0°$) or *trans* ($\omega = 180°$) configurations. Catalysis of bond rotation involves mechanisms that stabilize the relatively nonpolar transition state near the Syn-90 configuration ($\omega = 90°$) relative to the *cis* or *trans* ground states. Proposed mechanisms for this process in PPIases fall into three general classes: (1) the selective use of binding energy to stabilize the twisted, high-energy transition state and/or to destabilize the ground states (Harrison and Stein, 1990a; Fischer et al., 1993; Park et al., 1992), (2) the transfer of the isomerized peptide bond into a nonpolar environment through desolvation and hydrophobic interaction at the active site (Stein, 1993), and (3) the formation and stabilization of a tetrahedral geometry at the carbonyl carbon through formation of a covalent bond between enzyme and substrate (Fischer et al., 1989). Functional studies of cyclophilin- and FKBP-mediated prolyl isomerization show that only the first two proposed mechanisms contribute to the catalytic power of these enzymes (Park et al., 1992; Fischer et al., 1993).

Structural features of the Pin1 active site argue for all of these mechanisms during Pin1-mediated peptide bond isomerization. Modeling the rotation of a P.Ser-proline peptide bond built on the observed AlaPro dipeptide in the Pin1 active site demonstrates that the optimal geometry for interaction of the substrate i-1 anionic side chain with the Pin1 basic cluster is achieved with the Syn-90 conformation (Figure 6A). Interestingly, the crystallographically observed sulfate ion approaches within bonding distance of the $\beta$ carbon of the i-1 side chain during rotation, a finding that strongly suggests obligatory interaction of substrate with the basic cluster during bond rotation. This is fully consistent with the observed inhibition of Pin1 enzymatic activity against all tested tetrapeptide substrates by titration with inorganic phosphate (Figure 6C) or sulfate (not shown); binding of substrates and these multivalent anions must be mutually exclusive. Deprotonation of the basic cluster would reduce its overall positive charge. This would manifest itself catalytically only with interacting i-1 side

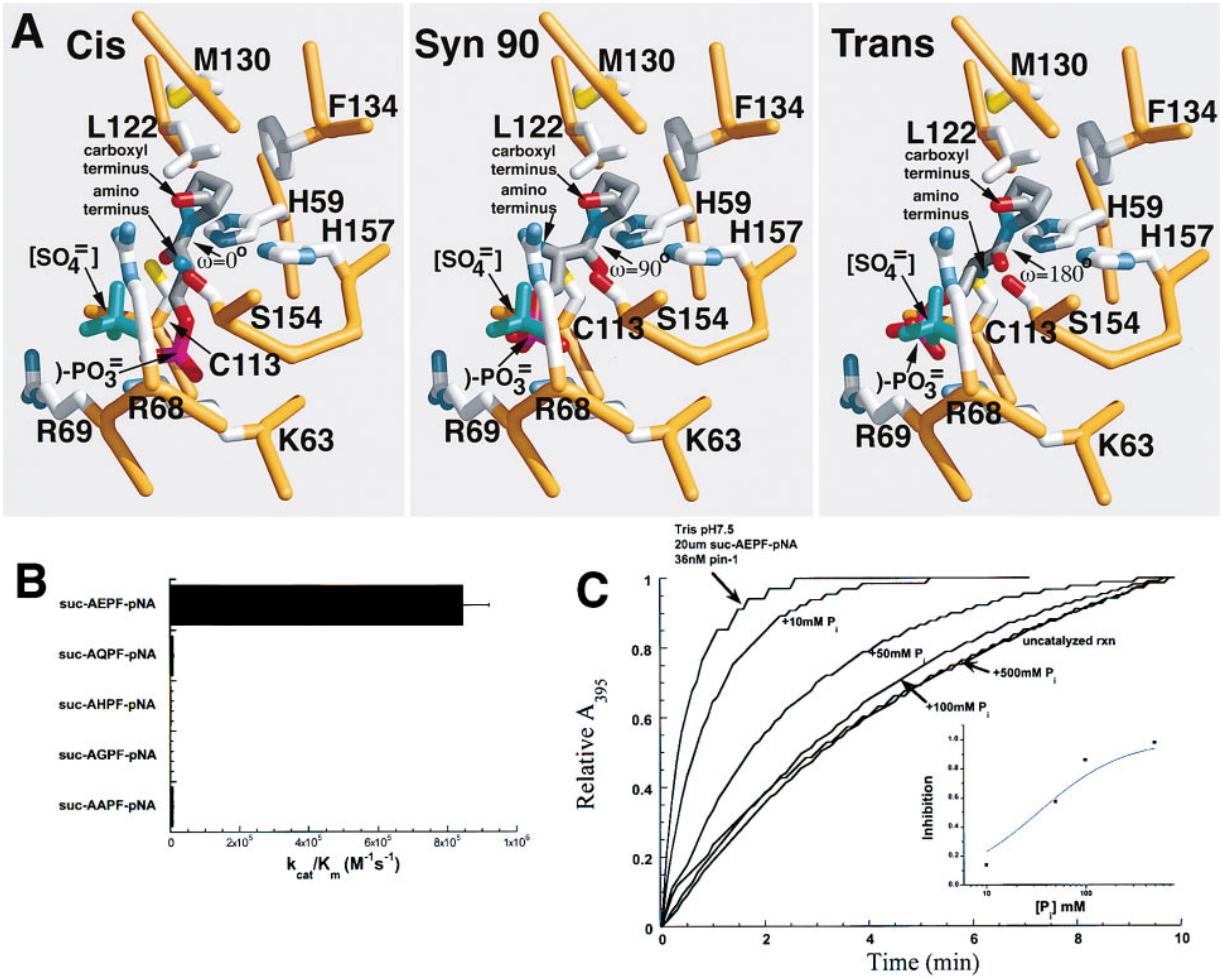


Figure 6. Substrate Specificity of the Pin1 PPIase

(A) Model for a phosphoserine-proline dipeptide bound to Pin1's active site. Atoms have been color coded for clarity. The P.Ser has been modeled on the original alanine in an extended low energy conformation with the N terminus pointing out of the active site. Rotations from *cis* through syn-90 to *trans* are counterclockwise when looking down the $C_{i-1}$-$N_i$ peptide bond. This rotation avoids passing the N terminus of the peptide through the Pin1 active site. The Syn-90 conformation results in maximal overlap of the extended P.Ser side chain with the bound sulfate. Steric clashes of the P.Ser side chain with the Pin1 active site in the *cis* or *trans* conformations would necessitate an active site rearrangement, and/or a transition of the P.Ser side chain to a higher energy conformation. Produced with the conic option (Huang et al., 1991) of MIDAS (Ferrin et al., 1988).

(B) A summary of chymotrypsin-coupled chromophoric PPIase assays using substrate peptides of the form succinyl-AlaXaa$_{i-1}$Pro$_i$Phe-(p)-nitroanilide, where Xaa is Ala, Gly, His, Gln, or Glu. $k_{cat}/K_m$ is plotted for each substrate, showing a greater than 100-fold preference for Glu over Gln at the i-1 position. $k_{cat}/K_m$ for all other residues tested are within 2-fold of that for Gln, with the exception of Gly, which shows no rate enhancement at any enzyme concentration tested.

(C) Inhibition of Pin1 PPIase activity by inorganic phosphate. Traces reflect Pin1 PPIase activity at a fixed concentration of Pin1 (36 nM) and succinyl-AlaGluProPhe-(p)-nitroanilide substrate (15 μM), with indicated concentrations of Pi. The single-binding isotherm (solid line) fits the data (dots) with an apparent $K_i$ of 33 mM.

chains. In concordance, Pin1 activity titrates down in the pH range 7.5–9.5 with suc-AEPF-pNA substrate, but not with suc-AAPF-pNA substrate (see Figure 7B, inset). Since titration in this pH range is an expected consequence of deprotonation of a lysine near other basic residues (Creighton, 1993), this result provides additional support for interaction of substrate with the active-site basic cluster.

The spatial arrangement of Cys-113, His-59, His-157, and Ser-154 relative to the isomerized peptide bond suggests a covalent catalytic mechanism unique to the Pin1 class of PPIase (Figure 7A). The initial step in the proposed scheme involves partial bond rotation by the favorable energetic forces described above (step 1, substrate shown in *cis* configuration). Coupled with the abstraction of a proton from Cys-113 by the deprotonated imidazole nitrogen of His-59, nucleophilic attack on the carbonyl carbon of the substrate peptide bond by the newly formed thiolate side chain takes place (step 2). This reaction leads to the establishment of a covalent tetrahedral intermediate between substrate and enzyme (step 3). The resulting negative charge on the former carbonyl oxygen is then stabilized through electrostatic interactions with a protonated His-157 (step 3). This

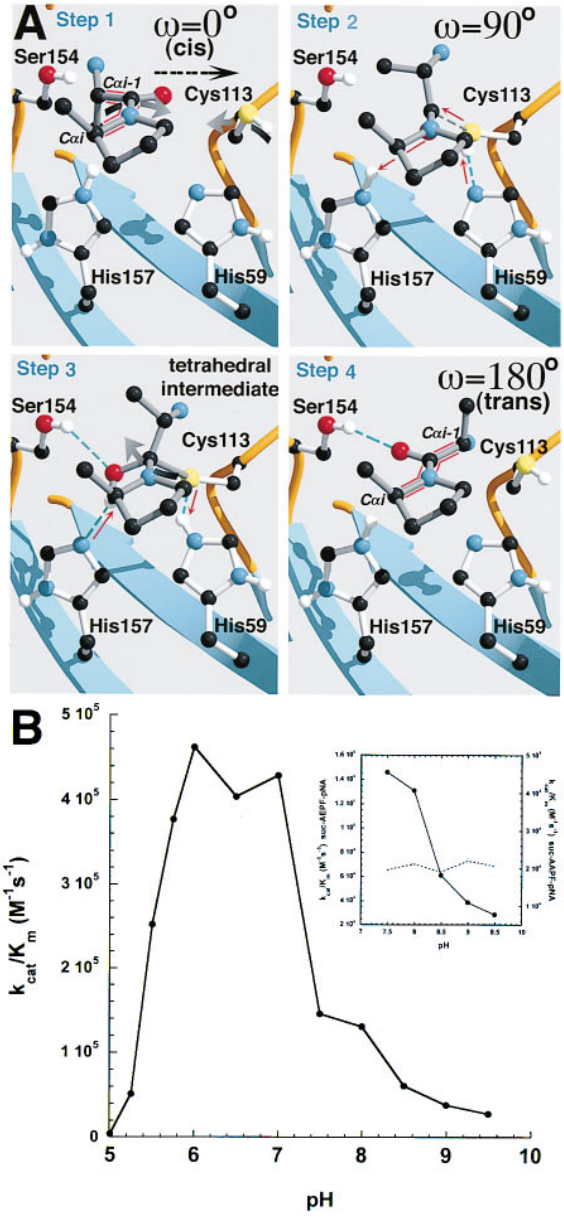


Figure 7. Pin1 PPIase Mechanism

(A) Model for Pin1's catalytic mechanism. Atoms are color coded for clarity. Hydrogen atoms have been included and are white. Dashed blue cylinders depict hydrogen bonds. Red arrows indicate the direction of the proposed electron flow. Gray arrows emphasize bond rotations. In the ground state, a steric clash between the thio group of Cys-113 and the carbonyl oxygen of the bound substrate prevents rotation of Cys-113's side chain into the active site cavity (step 1). Upon initial rotation of the peptide bond, Cys-113 moves into the active site and the substrate shifts to within bonding distance of the thiolate nucleophile (Step 2). Produced with MOLSCRIPT (Kraulis, 1991) and Raster3D (Bacon and Anderson, 1988). (B) Plot of $k_{cat}/K_m$ for Pin1 for its preferred substrate, suc-AEPF-pNA, as a function of pH. pH was adjusted to the indicated values with a mixed succinic acid/bis-Tris propane buffer. Unlike cyclophilin and FKBP, Pin1 displays a pH dependence, with apparent pKas consistent with titration of the active site His-59 and His-157. The inset shows titrations between pH 7.5 and 9.5 for suc-AEPF-pNA (closed circles, 36 nM Pin1) or for suc-AAPF-pNA (open circles, 1.2 μM Pin1), demonstrating that presence of the Glu side chain at the i-1 position confers pH sensitivity in this range. Lys-63 is a likely candidate for this titration.

high-energy intermediate relaxes back to either *cis* or *trans* ground states of the peptide bond (steps 1 or 4).

This reaction scheme involving a covalent intermediate implies two important properties. First, the catalytic process should require deprotonation of His-59 and should prefer the protonation of His-157, suggesting that unlike other classes of PPIase (Harrison and Stein, 1990a; Park et al., 1992), Pin1 activity should exhibit significant pH sensitivity. Indeed, Pin1 demonstrates a bell-shaped dependence on proton concentration, with activity increasing from zero to maximal with an apparent pKa of 5.6, and activity decreasing significantly with an apparent pKa of 7.5 (Figure 7B). The calculated pKas are well within the range expected for neighboring histidines in a protein environment (Creighton, 1993). Secondly, mutations at Cys-113 would be expected to decrease the catalytic activity of Pin1 by at least the fraction contributed by the covalent catalytic mechanism. Mutation of Cys-113 to Ala or Ser in Pin1 resulted in a 123-fold or 20-fold decrease in $k_{cat}/K_m$, respectively. Finally, as reported previously, the Pin1 triple mutant, G155A-H157A-I159A, failed to complement the *ess1*$^-$ mutation in vivo and lacked detectable PPIase activity against succinyl-AlaAlaProPhe-(p)-nitroanilide in vitro supporting a role for His-157 in the catalytic mechanism (Lu et al., 1996).

Together, these data support a model in which catalysis of bond rotation at the Pin1 active site progresses through the summed energetic contributions of distinct structural units. The contributions made by the overall hydrophobicity of the active site and the selective binding of conformationally strained substrate through interaction with the substrate selectivity filter are fully consistent with the overall fold similarity with FKBP and the conservation of the analogous structural motifs. In contrast to other PPIase structural classes, Pin1 appears to encode the additional property of covalent catalysis.

## Discussion

The proposed roles for PPIases involve the catalysis of protein folding or the trafficking of newly assembled proteins (Schmid, 1995). The original finding that the in vitro folding of ribonuclease A involves a mixture of slow and fast folding species differing in the isomeric state of prolyl peptide bonds prompted the hypothesis that catalysis of this isomerization would represent a general mechanism for accelerating protein folding in vivo. Direct evidence for PPIase-mediated cellular protein folding has been limited. Indirect evidence indicates that the formation of the collagen triple helix is limited by prolyl isomerizations and is facilitated by a cyclophilin-family PPIase (Steinmann et al., 1991). The mitochondrial cyclophilins from S. cerevisiae and N. crassa catalyze the refolding of proteins following mitochondrial import (Matouschek et al., 1995; Rassow et al., 1995). Evidence for the role of PPIases as molecular chaperones comes primarily from the visual system of Drosophila, where the photoreceptor cyclophilin, NinaA, which is essential for rhodopsin maturation, forms a complex with substrate rhodopsins (Colley et al., 1991; Baker et al., 1994) and may be involved in directing

rhodopsin from the endoplasmic reticulum to the sensory organelle known as the rhabdomere.

In addition to their activities on denatured or immature proteins, PPIases may also regulate fully folded proteins, for instance by accelerating peptidyl-prolyl bond isomerization. Resulting structural changes could affect the activity of target proteins. One mode by which a PPIase could regulate signaling protein activity is by accelerating the isomerization of surface prolines that are important components of intermolecular interaction surfaces. If a kinetic barrier between *cis*-*trans* XaaPro conformers that differ in biological activity exists, or if one of the structural conformers is unstable, then PPIase activity could effect a dramatic change in target protein activity. In addition, the possibility that the Pin1 PPIase domain preferentially recognizes a minimal segment consisting of a P.Ser (or P.Thr) N-terminal to proline would functionally link CDK activity and Pin1-catalyzed peptide bond isomerization, with CDK phosphorylation of Ser or Thr in the S/T-P segment of CDK targets promoting Pin1 interaction with CDK target proteins. Indeed, preliminary evidence shows that Pin1 specifically binds a subset of mitotic phosphoproteins in a phosphorylation-dependent manner (M. Shen and K. P. L., unpublished data). Thus, Pin1 may act in a general fashion during the cell cycle as a phosphorylation-dependent conformational switch for CDK targets.

Aspergillus NIMA, which interacts with human Pin1, exists as an oligomer both in vitro and in vivo (Lu et al., 1993), and this property is encoded within a ~100 amino acid segment of the large (~400 aa) noncatalytic C-terminal domain of NIMA (Lu and Hunter, 1995; M. Bowman et al., unpublished data). This segment inhibits NIMA function in a dominant manner when overexpressed (Lu and Hunter, 1995), suggesting a requirement for the oligomerized state of NIMA during cell cycle progression. The C-terminal SerPro/ThrPro–rich region of NIMA is sufficient for Pin1 binding (Lu et al., 1996) and is phosphorylated by CDC2 (Ye et al., 1995). Together, these findings suggest a model in which CDC2 phosphorylates NIMA at sites near the oligomerization domain to create an efficient substrate for Pin1. Pin1-mediated proline isomerization could lead to propagated structural alterations that destabilize the NIMA oligomer and cause changes in NIMA activity. Alternatively, such conformational changes could lead to altered localization of NIMA during the cell cycle through effects on structural motifs involved in protein–protein interactions.

Pin1 could also regulate cell cycle proteins stoichiometrically using binding energy to either stabilize high-energy conformations of target proteins, or to compete away other ligands. A similar proposal has been made for the human cyclophilin, CypA, by Schreiber and Crabtree (1992), who argue that CypA may not act as an enzyme in vivo and may instead mediate protein–protein interactions. The recent structure of the N-terminal domain of HIV-1 capsid with CypA illustrates this principle; CypA binding likely destabilizes the crystalline packing of capsid proteins, thereby leading to virion disassembly through the removal of key interaction sites (Gamble et al., 1996). This concept is consistent with the finding that Pin1 is found exclusively in a macromolecular complex in the nucleus (Lu et al., 1996) and thus might make high-affinity interactions with its targets possibly mediated through covalent interaction with Cys-113. While the C113A and C113S mutants possess measurable PPIase activity on synthetic tetrapeptides, they would clearly lack the ability to form covalent complexes. The study of the cell cycle phenotype of the Cys-113 mutants should clarify the biological role of this residue in mediating target interaction. The use of covalent interactions to stabilize an otherwise highly transient structural species with a partially twisted peptide bond might provide a highly efficient molecular switch, particularly if regulated by CDK phosphorylation. Structural studies of Pin1 complexes with native substrates and systematic mutagenesis of Pin1 residues implicated in catalysis and substrate recognition should help resolve the mechanism of Pin1-dependent cell cycle regulation.

## Experimental Procedures

### Expression and Purification of Pin1

N-terminally $His_6$-tagged Pin1 (Lu et al., 1996) was expressed at 22°C in E. coli strain BL21(DE3) following induction at an optical density of 1.2 (600 nM) with 0.4 mM IPTG for 4 hr in terrific broth. Cells were resuspended in 25 mM Tris–HCl (pH 8.0), 500 mM NaCl, 10 mM imidazole, 10 mM β-mercaptoethanol, and 1% (v/v) Tween 20 on ice (sonication buffer). Following sonication at 4°C, the soluble supernatant was loaded onto an Ni-NTA (Qiagen) column and washed with sonication buffer minus Tween 20. $His_6$Pin1 was eluted with 15 bed volumes of sonication buffer minus Tween 20 and supplemented with 250 mM imidazole. Eluted $His_6$Pin1 was digested with thrombin (Sigma) during dialysis for 12 hr at 4°C against 50 mM Tris–HCl (pH 8.0), 150 mM NaCl, 5 mM $MgCl_2$, 2.5 mM $CaCl_2$, 1 mM DTT, and 10% (v/v) glycerol, depleted of thrombin with a benzamidine-Sepharose column (Pharmacia), and fractionated by gel filtration on a Superdex 75 16/60 column (Pharmacia) equilibrated in 10 mM HEPES–$Na^+$ (pH 7.5), 100 mM NaCl, and 1 mM DTT. The Pin1-containing fractions were concentrated to 20 mg/ml with a Centricon-10 (Amicon) and stored at −80°C.

### Crystallization and Manipulation of Crystals

Crystals were grown in hanging drops at 4°C by mixing 5 μl of concentrated Pin1 (20 mg/ml) with 5 μl of a reservoir solution consisting of 2.00–2.50 M ammonium sulfate, 100 mM HEPES–$Na^+$ (pH 7.5), 1% (v/v) PEG400 (Sigma), and 1 mM DTT. Crystals appeared within 48 hr and grew to ~0.15 × 0.05 × 0.05 mm in 1–2 weeks. Microseeding was used to improve crystal size (typically 0.4 × 0.1 × 0.1 mm). Crystals were stabilized in 40% (v/v) PEG400, 50 mM HEPES–$Na^+$ (pH 7.5), and 1 mM DTT (stabilizer). The stabilized crystals were frozen in a stream of 100K nitrogen gas. The crystals contain one Pin1 molecule per asymmetric unit and belong to space group $P4_32_12$. Two crystal forms predominate; I: a = b = 47.6 Å, c = 134.9 Å, α = β = γ = 90°; II: a = b = 49.0 Å, c = 137.8 Å, α = β = γ = 90°. The complex of Pin1 with AlaPro dipeptide (AP II) was obtained by soaking a type II crystal in 40% (v/v) PEG400, 50 mM HEPES–$Na^+$ (pH 7.5), 50 mM $^+H_3N$-AlaPro-$COO^-$ (Sigma) for 48 hr at 4°C. A single site TAMM (tetrakis(acetoxymercuri)methane, Strem Chemical Inc.) derivative was obtained by soaking Pin1 crystals for 12 hr at 4°C in the stabilizer (minus DTT) saturated with TAMM. The five-site PIP (di-μ-iodobis(ethylenediamine)diplatinum(II)nitrate, Strem Chemicals Inc.) derivative was obtained by soaking Pin1 crystals for 48 hr at 4°C in the stabilizer (minus DTT) supplemented with 10 mM PIP.

### Data Collection and Structure Determination

Native (Nat I, 2.05 Å) and derivative data (2.5 Å) for crystal form I were collected on a MacScience imaging plate detector, DIP2020k (MacScience Corp.), using double focusing Pt/Ni–coated mirrors and Cu Kα X-rays from a MacScience M18XHF generator operating at 4.5 kW (50 kV × 90 mA). Data for Pin1 complexed with AlaPro dipeptide for crystal form II (AP II) were collected at the Stanford

Synchrotron Radiation Laboratory, beamline 7-1 ($\lambda$ = 1.08 Å) on a MAR imaging plate system. Data were processed with DENZO (Otwinowski, 1993) and scaled with SCALEPACK (Otwinowski, 1993). A single mercury binding site for the TAMM derivative was located on the isomorphous difference Patterson map and refined with ML-PHARE (Otwinowski, 1991). Subsequently, five platinum sites for the PIP derivative were located on difference Fourier maps using the TAMM-derived phases and corefined with the TAMM data in ML-PHARE. Solvent flattening, histogram matching, and Sayre's equation were employed to improve and extend phases to 2.05 Å resolution using DM (Cowtan, 1994). Model building was conducted with O (Jones et al., 1991), and the structures were refined with X-PLOR (Brunger, 1992). The initial native model (Nat I, residues 6–39, 45–163) was refined following partial solvent modeling (60 water molecules added) using all the data (no sigma cutoff) between 6.0 Å and 2.05 Å resolution. Subsequently, the Pin1 AlaPro complex (AP II) was solved using the Nat I model as a starting point for rigid body refinement in X-PLOR. Following positional and simulated annealing refinement, 208 water molecules, 2 PEG400 molecules, 1 sulfate ion, and 1 *cis* AlaPro dipeptide were modeled and refined with X-PLOR using all the data between 6.0 Å and 1.35 Å resolution. The crystallographic data are summarized in Table 1.

### Surface Hydrophobicity Analysis

The degree of conserved, solvent-exposed hydrophobicity for the ith residue was quantitatively assessed as a parameter $a_i$, defined as: $a_i$ = (conservation index)$_i$ (fractional solvent accessibility)$_i$ (hydrophobicity index)$_i$. A fractional conservation index was assigned for each Pin1 residue from the alignment with its functional homolog from yeast Ess1, where this index was taken as 0 for not conserved, 0.5 for chemically conserved, and 1 for identical. The solvent-accessible surface area for each residue was calculated using the CCP4 program RESAREA and was divided by the total surface area to give the fractional solvent accessibility. The hydrophobicity index is the ratio of the probability of finding a given residue in the interior to that on the surface ($P_i/P_o$) and is calculated as $e^{-\Delta G/RT}$ where the free energy is normalized such that $\Delta G_{Gly} = 0$ (Miller et al., 1987; Creighton, 1993). Values of $a_i$ were mapped onto a color scale and displayed on a molecular surface representation of Pin1 using GRASP (Nicholls et al., 1991).

### Site-Specific Mutagenesis and Kinetic Analysis

Site-directed mutations were introduced using PCR-based techniques and verified by automated sequencing. The corresponding proteins were expressed and purified as previously described. PPIase activity was measured by a protocol modified from Heitman et al. (1993) and Kofron et al. (1991). Purified Pin1 was diluted into assay buffer (50 mM succinic acid/bis–Tris propane at indicated pH values, 100 mM NaCl) immediately prior to kinetic measurements. A 900 $\mu$l cocktail containing Pin1 and 15–20 $\mu$M substrate was equilibrated in the spectrophotometer at 3.6°C. A chilled chymotrypsin (Sigma) solution (100 $\mu$l, 1 mM in water) was added, mixed for 5 s, and the absorbance of p-nitroaniline (at 395 nM) was followed every 6 s for 2–10 min. Total absorbance was normalized to zero immediately prior to data acquisition, and substrate concentration was adjusted to remain within the linear range of the instrument. Data were analyzed off-line using a combination of Excel 7.0 (Microsoft Corp.) and Origin 4.1 (Microcal Software). The PPIase rate-limited portion of each curve was well fit to a single exponential decay function of the form $1\text{-}ae_{bt}$, where a and b were free parameters. Goodness of fit was assessed by standard $\chi^2$ analyses. For inorganic phosphate inhibition assays, the indicated concentration of sodium phosphate buffer (pH 7.0) was added from a 1 M stock. Substrate peptides were from Bachem Inc.

### Acknowledgments

Correspondence regarding this paper should be addressed to J. P. N. We thank David Schultz and Charles Zuker for use of PPIase assay reagents; Hartmut Oschkinat for providing the YAP65 WW domain coordinates; Carl Hoeger for peptide synthesis; and Marianne Bowman, Eugene Lee, Matthew Harrington, and Michael Reese for technical assistance. We thank Courtney Starks, Alexandrine Bilwes, and the staff of the Stanford Synchrotron Radiation Laboratory for assistance at beamline 7-1. The work performed was supported by the NIH and DOE (SSRL) and in part by funds from the Lucille P. Markey Charitable Trust (J. P. N.) and USPHS grant CA54418 (J. P. N.). R. R. was a Burroughs-Wellcome Fund Fellow of the Life Sciences Research Foundation. K. P. L. was a Leukemia Society of America Fellow, and T. H. is an American Cancer Society Research Professor. Correspondence and requests for materials should be addressed to J. P. N. Until deposition in the Brookhaven Protein Data Bank, coordinates can be obtained from the following e-mail address: Noel@sbl.salk.edu.

Received March 20, 1997; revised May 6, 1997.

### References

Albers, M.W., Walsh, C.T., and Schreiber, S.L. (1990). Substrate specificity for the human rotamase FKBP: a view of FK506 and rapamycin as leucine-(twisted amide)-proline mimics. J. Org. Chem. *55*, 4984–4986.

Bacon, D., and Anderson, W.F. (1988). A fast algorithm for rendering space-filling molecule pictures. J. Mol. Graphics *6*, 219–220.

Baker, E.K., Colley, N.J., and Zuker, C.S. (1994). The cyclophilin homolog ninaA functions as a chaperone, forming a stable complex in vivo with its protein target rhodopsin. EMBO J. *13*, 4886–4895.

Brunger, A.T. (1992). X-PLOR Version 3.1: A System for X-Ray Crystallography and NMR (New Haven, Connecticut: Department of Molecular Biophysics and Biochemistry and Howard Hughes Medical Institute, Yale University).

Carson, M., and Bugg, C.E. (1986). Algorithm for ribbon models of proteins. J. Mol. Graphics *4*, 121–122.

Chan, D.C., Bedford, M.T., and Leder, P. (1996). Formin binding proteins bear WWP/WW domains that bind proline-rich peptides and functionally resemble SH3 domains. EMBO J. *15*, 1045–1054.

Clackson, T., and Wells, J.A. (1995). A hot spot of binding energy in a hormone-receptor interface. Science *267*, 383–386.

Colley, N.J., Baker, E.K., Stamnes, M.A., and Zuker, C.S. (1991). The cyclophilin homolog ninaA is required in the secretory pathway. Cell *67*, 255–263.

Cowtan, K.D. (1994). 'dm': an automated procedure for phase improvement by density modification. Joint CCP4 and ESF-EACBM Newsletter on Protein Crystallography *31*, pp. 34–38.

Creighton, T.E. (1993). Proteins Structures and Molecular Properties (New York: W.H. Freeman and Company).

Ferrin, T.E., Huang, C.C., Jarvis, L.E., and Langridge, R. (1988). The MIDAS display system. J. Mol. Graphics *6*, 13–27.

Fischer, G., Wittmann-Liebold, B., Lang, K., Kiefhaber, T., and Schmid, F.X. (1989). Cyclophilin and peptidyl-prolyl *cis-trans* isomerase are probably identical proteins. Nature *337*, 476–478.

Fischer, S., Michnick, S., and Karplus, M. (1993). A mechanism for rotamase catalysis by the FK506 binding protein (FKBP). Biochemistry *32*, 13830–13837.

Gamble, T.R., Vajdos, F.F., Yoo, S., Worthylake, D.K., Houseweart, M., Sundquist, W.I., and Hill, C.P. (1996). Crystal structure of human cyclophilin A bound to the amino-terminal domain of HIV-1 capsid. Cell *87*, 1285–1294.

Hanes, S.D., Shank, P.R., and Bostian, K.A. (1989). Sequence and mutational analysis of ESS1, a gene essential for growth in *Saccharomyces cerevisiae*. Yeast *5*, 55–72.

Harrison, R.K., and Stein, R.L. (1990a). Mechanistic studies of peptidyl prolyl *cis-trans* isomerase: evidence for catalysis by distortion. Biochemistry *29*, 1684–1689.

Harrison, R.K., and Stein, R.L. (1990b). Substrate specificities of the peptidyl prolyl *cis-trans* isomerase activities of cyclophilin and FK-506 binding protein: evidence for the existence of a family of distinct enzymes. Biochemistry *29*, 3813–3816.

Heitman, J., Koller, A., Cardena, M.E., and Hall, M.N. (1993). Identification of immunosuppressive drug targets in yeast. METHODS: A Companion to Methods in Enzymology *5*, 176–187.

Hemenway, C.S., and Heitman, J. (1996). Immunosuppressent target protein FKBP12 is required for P-glycoprotein function in yeast. J. Biol. Chem. *271*, 18527–18534.

Huang, C.C., Petersen, E.F., Klein, T.E., Ferrin, T.E., and Langridge, R. (1991). Conic: a fast renderer for space-filling molecules with shadows. J. Mol. Graphics *9*, 230–236.

Janin, J., and Chothia, C. (1990). The structure of protein–protein recognition sites. J. Biol. Chem. *265*, 16027–16030.

Jones, T.A., Zou, J.Y., Cowan, S., and Kjeldgaard, M. (1991). Improved methods for building protein models in electron density maps and the location of errors in these models. Acta Crystallogr. *A47*, 110–119.

King, R.W., Jackson, P.K., and Kirschner, M.W. (1994). Mitosis in transition. Cell *79*, 563–571.

Kofron, J.L., Kuzmic, P., Kishore, V., Colon-Bonilla, E., and Rich, D.H. (1991). Determination of kinetic constants for peptidyl prolyl *cis-trans* isomerases by an improved spectrophotometric assay. Biochemistry *30*, 6127–6134.

Kraulis, P. (1991). MOLSCRIPT: a program to produce both detailed and schematic plots of protein structures. J. Appl. Crystallogr. *24*, 946–950.

Lu, K.P., and Hunter, T. (1995). Evidence for a NIMA-like mitotic pathway in vertebrate cells. Cell *81*, 413–424.

Lu, K.P., and Means, A.R. (1994). Expression of the noncatalytic domain of the NIMA kinase causes a G2 arrest in *Aspergillus nidulans*. EMBO J. *13*, 2103–2113.

Lu, K.P., Osmani, S.A., and Means, A.R. (1993). Properties and regulation of the cell cycle–specific NIMA protein kinase of *Aspergillus nidulans*. J. Biol. Chem. *268*, 8769–8776.

Lu, K.P., Hanes, S.D., and Hunter, T. (1996). A human peptidyl-prolyl isomerase essential for regulation of mitosis. Nature *380*, 544–547.

Macias, M.J., Hyvonen, M., Baraldi, E., Schultz, J., Sudol, M., Saraste, M., and Oschkinat, H. (1996). Structure of the WW domain of a kinase-associated protein complexed with a proline-rich peptide. Nature *382*, 646–649.

Matouschek, A., Rospert, S., Schmid, K., Glick, B.S., and Schatz, G. (1995). Cyclophilin catalyzes protein folding in yeast mitochondria. Proc. Natl. Acad. Sci. USA *92*, 6319–6323.

Miller, S., Janin, J., Lesk, A.M., and Chothia, C. (1987). Interior and surface of monomeric proteins. J. Mol. Biol. *196*, 641–656.

Nicholls, A., Sharp, K.A., and Honig, B. (1991). Protein folding and association: insights from the interfacial and thermodynamic properties of hydrocarbons. Proteins *11*, 281–296.

Nurse, P. (1994). Ordering S phase and M phase in the cell cycle. Cell *79*, 547–550.

Osmani, A.H. McGuire, S.L., and Osmani, S.A. (1991) Parallel activation of the NIMA and p34cdc2 cell cycle–regulated protein kinases is required to initiate mitosis in *A. nidulans*. Cell *67*, 283–291.

Otwinowski, Z. (1991). ML-PHARE (Warrington, England: Science and Engineering Research Council Collaborative Computing Project Number 4, Daresbury Laboratory).

Otwinowski, Z. (1993). Oscillation data reduction program. In Data Collection and Processing, L. Sawyer, N. Issacs, and S. Bailey, eds. (Warrington, England: Science and Engineering Research Council, Daresbury Laboratory), pp. 55–62.

Park, S.T., Aldape, R.A., Futer, O., DeCenzo, M.T., and Livingston, D.J. (1992). PPIase catalysis by human FK506-binding protein proceeds through a conformational twist mechanism. J. Biol. Chem. *267*, 3316–3324.

Rassow, J., Mohrs, K., Koidl, S., Barthelmess, I.B., Pfanner, N., and Tropschug, M. (1995). Cyclophilin 20 is involved in mitochondrial protein folding in cooperation with molecular chaperones Hsp70 and Hsp60. Mol. Cell. Biol. *15*, 2654–2662.

Schmid, F.X. (1995). Prolyl isomerases join the fold. Curr. Biol. *5*, 993–994.

Schreiber, S.L., and Crabtree, G.R. (1992). The mechanism of action of cyclosporin A and FK506. Immunol. Today *13*, 136–142.

Staub, O., and Rotin, D. (1996). WW domains. Structure *4*, 495–499.

Stein, R.L. (1993). Mechanism of enzymatic and nonenzymatic prolyl cis-trans isomerization. Adv. Prot. Chem. *44*, 1–24.

Steinmann, B., Bruckner, P., and Supertifurga, A. (1991). Cyclosporin-A slows collagen triple-helix formation in vivo—indirect evidence for a physiologic role of peptidyl-prolyl *cis-trans*-isomerase. J. Biol. Chem. *266*, 1299–1303.

Sudol, M. (1996a). Structure and function of the WW Domain. Prog. Biophys. Mol. Biol. *65*, 113–132.

Sudol, M. (1996b). The WW module competes with the SH3 domain? Trends Biochem. Sci. *21*, 161–163.

Sudol, M., Chen, H.I., Bougeret, C., Einbond, A., and Bork, P. (1995). Characterization of a novel protein-binding module—the WW domain. FEBS Lett. *369*, 67–71.

Van Duyne, G.D., Standaert, R.F., Karplus, P.A., Schreiber, S.L., and Clardy, J. (1993). Atomic structures of the human immunophilin FKBP-12 complexes with FK506 and Rapamycin. J. Mol. Biol. *229*, 105–124.

Ye, X.S., Xu, G., Pu, R.T., Fincher, R.R., McGuire, S.L., Osmani, A.H., and Osmani, S.A. (1995). The NIMA protein kinase is hyperphosphorylated and activated downstream of p34cdc2/cyclin B: coordination of two mitosis promoting kinases. EMBO J. *14*, 986–994.

Young, L., Jernigan, R.L., and Covell, D.G. (1994). A role for surface hydrophobicity in protein–protein recognition. Prot. Sci. *3*, 717–729.